PHOTONICS Research

All-fiber spatiotemporal mode-locking lasers with large modal dispersion

Huaiwei Zhang,[1] Yunhong Zhang,[1] Jiying Peng,[1,*] Xinyang Su,[1] Xiaosheng Xiao,[2] Dongjian Xu,[1] Junhao Chen,[1] Tianran Sun,[1] Kai Zheng,[1] Jianquan Yao,[1] and Yi Zheng[1]

[1]Key Laboratory of Luminescence and Optical Information, Ministry of Education, Beijing Jiaotong University, Beijing 100044, China
[2]State Key Laboratory of Information Photonics and Optical Communications, School of Electronic Engineering, Beijing University of Posts and Telecommunications, Beijing 100876, China
*Corresponding author: jypeng@bjtu.edu.cn

Received 1 October 2021; revised 5 December 2021; accepted 9 December 2021; posted 13 December 2021 (Doc. ID 444750); published 1 February 2022

It is a challenging problem to balance the modal walk-off (modal dispersion) between multiple transverse modes and chromatic dispersion in long step-index multimode fibers (MMFs). By properly designing the oscillator, we have overcome the difficulty and successfully obtained an all-fiber spatiotemporal mode-locked laser based on step-index MMFs with large modal dispersion for the first time, to our knowledge. Various proofs of spatiotemporal mode-locking (STML) such as spatial, spectral, and temporal properties, are measured and characterized. This laser works at a fundamental frequency of 28.7 MHz, and achieves a pulse laser with single pulse energy of 8 nJ, pulse width of 20.1 ps, and signal-to-noise ratio of ~70 dB. In addition, we observe a dynamic evolution of the transverse mode energy during the STML establishment process that has never been reported before.

https://doi.org/10.1364/PRJ.444750

1. INTRODUCTION

Mode-locked (ML) lasers have vital applications in biomedical therapies, scientific research, terahertz-wave generation, industry, etc [1,2]. Fiber lasers operating in single transverse mode have become a considerable platform for achieving mode-locking due to their compact structure, flexible transmission, and excellent spatial beam profiles. Therefore, they have gone through extensive and in-depth investigations. Many outstanding performances, such as ultra-short pulse width and ultra-low noise, have been achieved in single-transverse-mode fiber lasers [3,4]. However, under moderate peak power, a small fiber core will induce a strong nonlinear effect, and the accumulation of nonlinear phase will break the pulse and restrict further improvement of the energy [5]. Furthermore, in the current era of data explosion, the transmission of large amounts of data is also a great challenge for single-mode fibers (SMFs). Naturally, researchers expect that multimode fibers (MMFs) with large core diameters can solve these problems.

In fact, MMF even predates SMF. Yet, the broad bandwidth and structural simplicity of SMF have reduced researchers' interest in MMF [6]. In the last few years, MMF has renewed the attention of researchers. MMF possesses a larger mode area and an additional spatial degree of freedom; consequently, it is an ideal platform for studying high-dimensional complex spatiotemporal nonlinear dynamics [7]. Numbers of novel nonlinear phenomena such as nonlinear MM interference (NL-MMI) [8,9], spatial beam cleaning [10–13], spatiotemporal instability [14,15], optical solitons [16–19], and controllable spatiotemporal nonlinear effects [5,6], have been discovered and studied. In the field of laser transmission, MMF is also widely used for flexible transmission of high-energy lasers, but it is rarely reported that MMF with meter-level length was used in a resonant cavity to achieve MM ML pulse output before 2017.

In 2017, Wright *et al.* took advantage of graded-index (GRIN) MMF in an oscillator and realized the spatiotemporal mode-locking (STML) pulsed laser, by locking the transverse and longitudinal modes simultaneously [3]. Wright *et al.* pointed out the key factor to achieve STML was to control the modal dispersion. Through strong spectral filtering and spatial filtering, modal dispersion and chromatic dispersion can be counteracted, thereby allowing transverse modes to be transmitted together along with the fiber. Generally, GRIN MMF holds an approximate parabolic refractive index distribution, and it has smaller modal dispersion than step-index (STIN) MMF [7,20]. Therefore, it is easy to achieve the balance of dispersion. The emergence of STML lasers opened up a new direction for the study of high-dimensional nonlinear dynamics and laser applications [3,21,22]. Very recently, Ding *et al.* demonstrated that STML could also be achieved in MMF lasers with large modal dispersion [7]. A short active STIN MMF is fusion spliced with a relatively long GRIN MMF and then

combined with a free-space structure to form an STML fiber laser. The result proves the possibility of using the STIN MMF with large modal dispersion in STML fiber lasers. Then, how to build a low-cost all-fiber STML laser based on STIN MMF with large modal dispersion is the next challenging task.

Since the unavailability of active GRIN MMF, and the traditional quasi-single-mode active fiber limits the dimensions of nonlinear dynamics and the potential performance of the laser, the use of commercially available active STIN MMF is more practical. In addition, the use of transmission fibers that match the active STIN MMF will also effectively reduce the accumulation of nonlinear phases in the fiber and enhance the output energy of the lasers. Furthermore, all-fiber lasers remove the free-space elements in the resonant cavity, eliminating the intracavity air gap [23,24]. The all-fiber structure is stable and compact, easily achieves high-gain and high-power output, and is preferred for practical applications [25]. However, it is worth noting that when multiple transverse modes are transmitted in the long STIN MMF, more modal walk-off will be generated (see Appendix A), which is difficult to compensate for. This means that achieving STML in an all-fiber oscillator (mainly composed of STIN fibers) with large modal dispersion is a challenge.

Nonetheless, by rationally designing the oscillator, there is a possibility to solve the above problems. In all-fiber MM lasers, an oscillator containing GRIN MMF, long passive STIN MMF, and active STIN MMF with large modal dispersion is designed. With a saturable absorber (SA), served by nonlinear polarization rotation (NPR) and a spectral filter based on NL-MMI, we successfully realize the self-starting STML after reaching the mode-locking threshold. By splicing spectral filters after GRIN MMF, the functions of virtual spatial filtering and spectral filtering are cleverly realized simultaneously, which plays a key role in the formation of STML. We perform the corresponding numerical simulation investigation on the all-fiber cavity. The results verify that spatial filtering effectively balances modal dispersion during the STML process in our cavity. Since MM ML lasers are expected to increase pulse energy by two orders of magnitude [3], our design provides a significant value for the realization of all-fiber high-power ML pulsed lasers in the future.

2. EXPERIMENTAL SETUP

The experimental setup diagram is shown in Fig. 1. The active fiber used in the experiment is a segment of STIN MMF (Nufern LMA-YDF-20/125-9M) with a 20 μm core diameter and numerical aperture (NA) = 0.08, where ~6 modes are supported. The GRIN MMF is produced by Corning corporation with a 50 μm core diameter and NA = 0.2. The role of GRIN MMF is to induce a strong SA effect through the accumulation of NPR, which contributes to the formation of STML. In addition, this section fusion splicing with the next part of the fiber constitutes a virtual spatial filter. The STIN ytterbium-doped fiber (YDF) and GRIN MMF are spliced together, and the higher-order modes (HOMs) in GRIN MMF are excited by the active fiber. The other fibers are pigtails of the device, and the pigtails are passive STIN fibers (Nufern LMA-GDF-20/125-M, 20 μm core diameter, NA = 0.08) precisely matched with YDF.

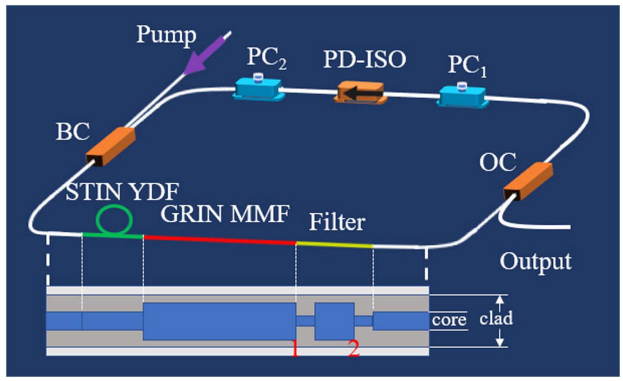

Fig. 1. Experiment setup. BC, beam combiner; STIN YDF, step-index ytterbium-doped fiber (Nufern LMA-YDF-20/125-9M); GRIN MMF, graded-index multimode fiber (Corning, 50/125); filter, spectral filter; OC, optical coupler (10% output); PC, polarization controller (PC_1, PC_2); PD-ISO, polarization-dependent isolator; pigtail fiber, passive step-index fiber matched with YDF (Nufern LMA-GDF-20/125-M).

The pump light is coupled into the ring cavity through the beam combiner (BC). The pump source is a semiconductor laser with a center wavelength of 976 nm. A 90:10 MM optical coupler (OC) is inserted, by which 10% of the average output power is reflected from the cavity for monitoring laser performance.

In normal dispersion ML fiber lasers, the spectral filter is regularly applied to meet the requirement of pulse self-consistency [26]. Therefore, we make a bandpass filter with a bandwidth of 10 nm and splice it behind the GRIN MMF [27,28]. The structure of the filter is composed of SMF-MMF-SMF. In this experiment, the SMF in the filter adopts the fiber with a core diameter of 10 μm (Nufern LMA-GDF-10/125-M). This fiber supports about three modes and should be actually regarded as a few-mode fiber. The artificial SA is composed of two polarization controllers (PCs) and a polarization-dependent isolator (PD-ISO). According to the NPR mechanism, nonlinear loss is realized [29].

The lengths of active fiber, GRIN MMF, and filter are 73.5 cm, 103 cm, and 38 cm, respectively. The total length of the ring cavity is about 7.2 m. The entire device is loosely placed on the platform to ensure HOM transmission. In addition, the group velocity dispersion (GVD) of GRIN MMF and STIN MMF at 1030 nm can be calculated according to their specifications. The GVD values of the six lowest-order modes of STIN MMF and GRIN MMF are about 18.5–23.2 fs^2/mm and 18.8–18.9 fs^2/mm, respectively. For mode 1, the rough value of the cavity GVD is ~0.1338 ps^2.

The pulse train is detected by a 5 GHz bandwidth fast InGaAs photodetector (Thorlabs, DET08C/M) and a 3 GHz bandwidth digital oscilloscope (LeCroy WavePro 7300A). The spectrum is measured by an optical spectrum analyzer (ANDO, AQ6317B). A radio-frequency (RF) analyzer (Agilent, N9020A) ranging from 10 Hz to 3.6 GHz is used to study the output pulse sequence in the frequency domain.

3. RESULTS AND DISCUSSION

A. All-Fiber STML Lasers

After the experimental device shown in Fig. 1 is assembled, the PCs are adjusted to a proper position. With the increase in pump power, the laser experiences an incomplete modulated state before reaching the STML. It appears that several pulse envelopes are similar to *Q*-switched mode-locking (QSML) envelopes. They are randomly selected and detected through an oscilloscope to monitor the pulse train on a small scale, and it is found that the laser works at the fundamental frequency that matches the cavity length. However, it does not conform to the characteristics of QSML. Due to the insertion of the filter and PC, the threshold for mode-locking is relatively high. When the pump power reaches 5 W, the self-starting of STML is realized. The stable STML can be kept until the pump power is increased to 13.7 W, and the output power is also raised accordingly. After filtering the cladding power, the measured output power goes up to 232.2 mW. The average output power change varying with pump power is shown in Fig. 2(a). The slope efficiency of the laser is 1.75%. The output power deviation at each pump power is also recorded. According to the experiment results, the largest deviation is less than 1 mW. When the pump power varies from high to low, the ML state remains stable. Figure 2(b) presents the typical pulse train under 5 μs/div monitored by the oscilloscope at the pump power of 8.6 W. We randomly select a section of Fig. 2(b) and display it as Fig. 2(c). In terms of stability, this laser can continuously maintain STML stable operation for 12 h at room temperature (only 12 h test has been performed). When the pump power exceeds 13.7 W, if the PC is in a suitable position, a transition from mode-locking to QSML occurs (see Appendix B). Recently, some research groups have reported on the research of transition states in MMF lasers, such as QSML and the transition between *Q*-switching and STML [30,31]. However, this is the first demonstration of the transition from mode-locking to QSML in MM lasers. Before this paper, it has been reported in only SM ML lasers [32]. The research and explanation of the above phenomena are still in progress.

For STML, the beam profiles are a very important means of characterization, so we measured the beam profile by a CCD camera (Spiricon BGS-USB-SP928-OSI). In addition, spatial sampling is introduced to characterize the spectrum and RF spectral and temporal characteristics at the corresponding beam spot position.

Figures 3(a) and 3(d) display the beam profiles before STML and during the STML state, and it is obvious that the beam profiles have undergone obvious changes. Figures 3(b) and 3(e) show the beam intensity distribution before and during STML more clearly from the 3D perspective. At a fixed pump power and other cavity parameters, the spatial beam profile displays stationary spatial distributions before and after STML. The beam profiles in different states are spatially sampled, and the spectral information obtained is shown in Figs. 3(c) and 3(f). Before STML occurs, the spectrum width is narrow. At the state of STML, the spectrum width becomes broadened. Two sampled spots have different frequency components, and this confirms the existence of different transverse modes [7]. The significant changes in temporal, spatial, and spectral characteristics before and during ML confirm that STML is realized [3,7]. Figures 3(g) and 3(h) demonstrate the pulse train and RF spectrum at different positions of the beam during STML, respectively, which show that different transverse modes are ML and working at the fundamental repetition rate.

Figure 4(a) is the autocorrelation (AC) trace measured by the intensity autocorrelator (Femtochrome, FR-103XL). Assuming a profile of sech^2 shape, the AC trace indicates that the pulse width is 20.1 ps. Figure 4(b) shows the signal-to-noise ratio (SNR) with 10 Hz resolution bandwidth and 50 kHz span up to ~70 dB, which indicates a high stability of operation. The inset of Fig. 4(b) is the RF spectrum over a 1 GHz span, proving a uniform intensity pattern. The STML fiber laser is operating at a fundamental frequency of 28.7 MHz, which matches the cavity length. Figure 4(c) is a comparison diagram of the overall output spectrum during and before STML measured on a linear scale. During STML, the full width at half maximum (FWHM) reaches 24 nm. We also measure the overall output spectrum during STML on the log scale, as shown in Fig. 4(d). The inset in Fig. 4(d) shows the spectrum with 0.01 nm resolution over a 0.35 nm span, and we can find that the spectrum is modulated due to interference between multiple transverse modes [3,33].

In this all-fiber cavity with long STIN fibers, the transmission of different transverse modes in the fiber will induce

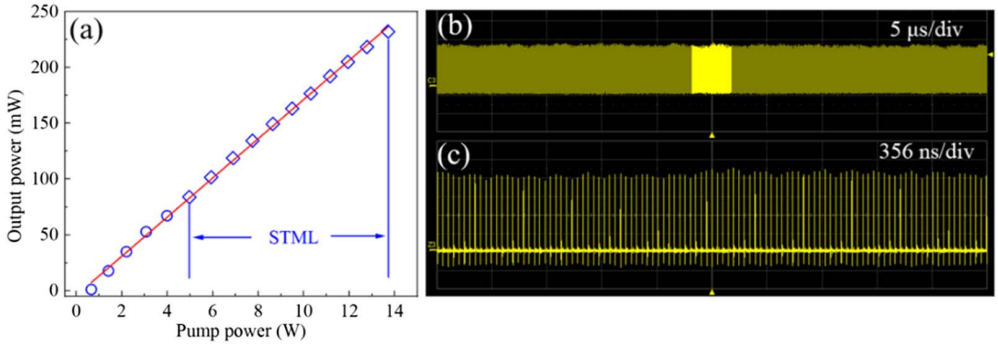

Fig. 2. (a) Average output power versus pump power. The red line is a linear fit to show laser efficiency. STML, spatiotemporal mode-locking. The laser is in STML operation in the marked range. Typical pulse train under (b) 5 μs/div and (c) 356 ns/div monitored by the oscilloscope at a pump power of 8.6 W.

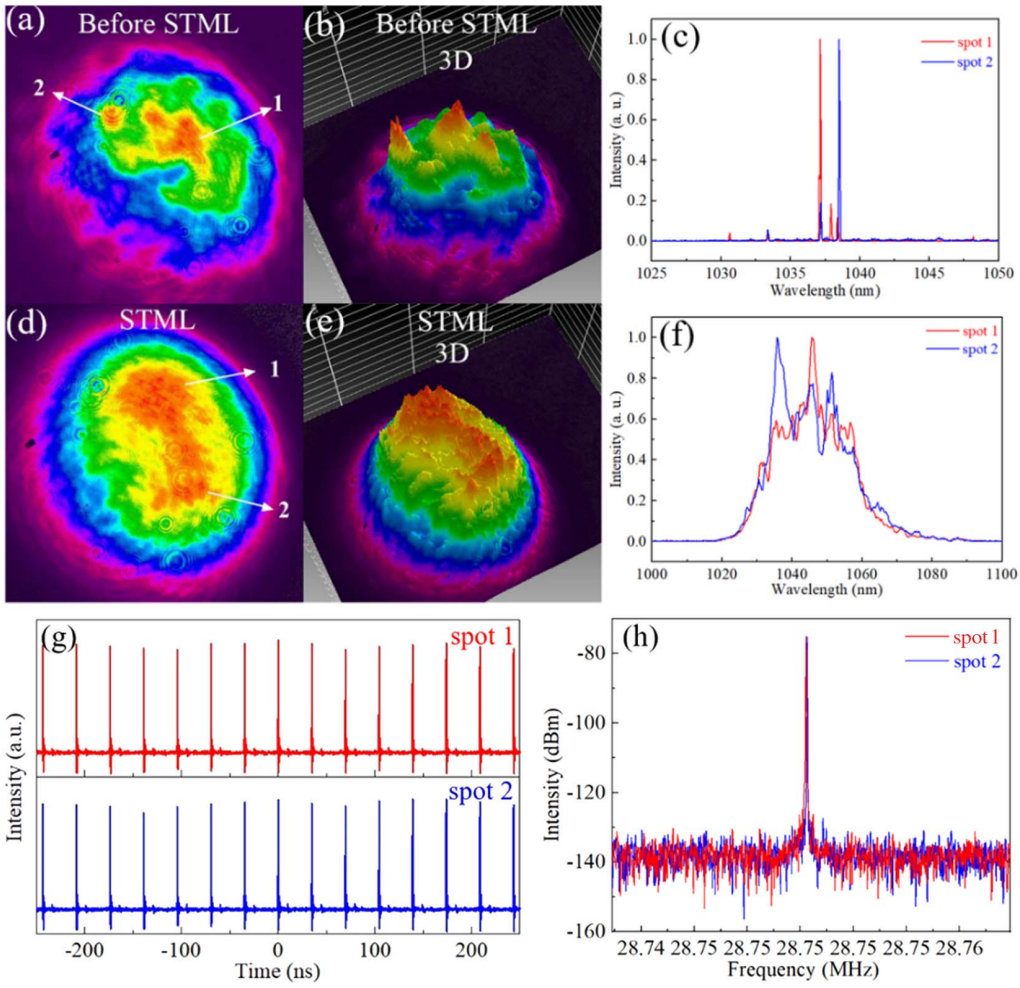

Fig. 3. Various proofs of STML. (a) 2D and (b) 3D beam profiles before STML. (c) Spectrum corresponding to different sampling points (1, 2) before STML. (d) 2D and (e) 3D beam profiles during STML. (f) Spectrum, (g) pulse train, and (h) RF spectrum corresponding to different sampling points (1, 2) during STML.

more modal walk-off (due to the large modal dispersion). As mentioned in Ref. [3] and Ref. [7], the important factor for achieving STML in a cavity with large modal dispersion is to balance chromatic dispersion and walk-off among transverse modes. The artificial SA and fiber-based filters implemented in this experiment jointly fulfill the above requirements. The artificial SA has two functions: one is to generate nonlinear loss to realize its basic function by the evolution of the polarization state, and the other is the effective balance of the walk-off between transverse modes. Filters also play two important roles: one is to bring about spectral filtering and to achieve pulse self-consistency in a cycle, and the other is to play the role of a virtual spatial filtering action. The formation of STML pulses in all-fiber lasers based on STIN fibers with large modal dispersion is closely related to this effect, as shown in the following simulation. As we all know, the fiber-based filter is composed of SMF-MMF-SMF [28], and the huge difference between the fiber core diameters and NAs makes a strong spatial filtering effect at the fusion splice point. Since the filter follows the MMF, there are two fusion points of MMF-SMF, as shown in Fig. 1. This makes the spatial filtering effect greatly enhanced. The cooperation of filter and SA makes the transverse and longitudinal modes locked together in each cycle to realize STML.

To verify the role of the fiber-based filter in the STML process, a corresponding numerical investigation on the all-fiber cavity is performed. A typical numerical result that shows the intracavity evolution of the modal walk-off of the steady STML state is presented in Fig. 5 (for additional simulation details, see Appendix C). Unlike the case of Ref. [7] where the modal dispersion was mainly compensated for by SA, in our cavity, the compensation of walk-off among the modes can be mainly attributed to virtual spatial filtering, which occurs on the coupling from the GRIN MMF into the fiber-based spectral filter. This effect of spatial filtering on modal dispersion compensation is similar to that in an STML MM Mamyshev oscillator observed recently [34].

B. Additional Phenomena

In the experiment, we observe that when increasing only the pump power without moving any other parts, the intensity changes in different transverse modes in the output beam

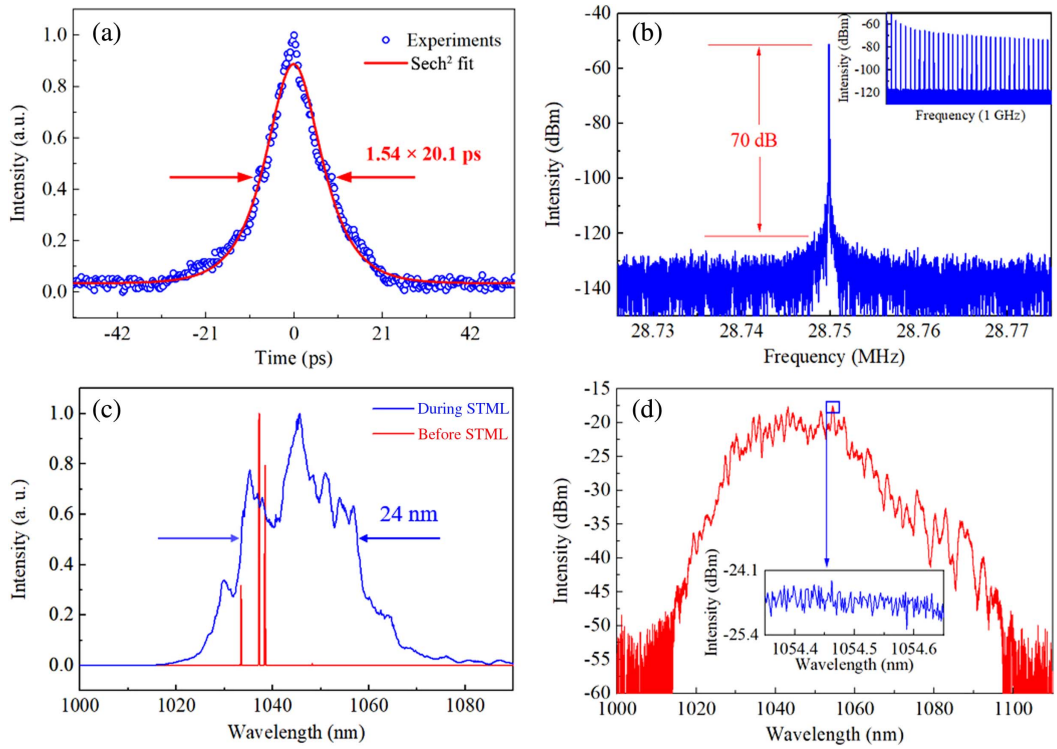

Fig. 4. Various output parameters of STML fiber laser. (a) Autocorrelation trace. (b) RF spectrum with 10 Hz resolution bandwidth and 50 kHz span; the inset is the RF spectrum over a 1 GHz span and 51 Hz resolution. (c) Measured spectrum in linear scale before STML and during STML. (d) Measured spectrum in log scale during STML; the inset is a detailed image at a center wavelength of 1054.5 nm, with a resolution of 0.01 nm.

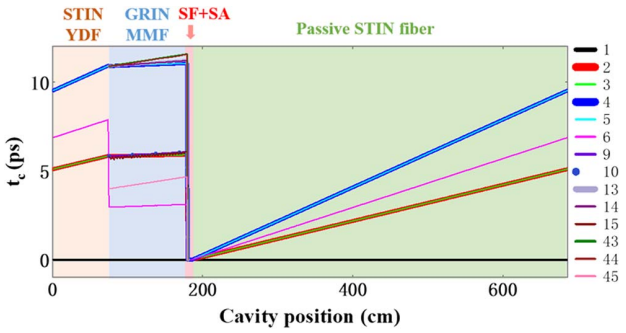

Fig. 5. Intracavity evolution of the walk-off among spatial modes. The walk-off is represented by the temporal center of gravity (t_c) for all considered modes relative to the fundamental mode (mode 1) in each fiber. Regions in orange, blue, red, and green represent the MM gain fiber, MM passive GRIN fiber, spectral filter (as well as a virtual spatial filter) and SA, and passive MM fiber, respectively. STIN, step-index; YDF, Yb-doped fiber; GRIN MMF, graded-index multi-mode fiber; SF + SA, spectral filter and saturable absorber. All six modes in the STIN fibers and modes 1–6, 9, 10, 13–15, and 43–45 in the GRIN MMF are considered in the simulations. The colors for the modes are the same for all fibers, as shown in the legend. Note that the curves of modes 2 and 3, and modes 4 and 5, etc., overlap.

are different during the whole process of STML establishment. Before the establishment of STML, the increasing of pump power increases only the intensity of a few modes. Similar to the degeneration of beam propagation into speckle distortion in MMF, the beam profile distribution is irregular before the STML state. When STML is established, a sudden change in the beam profile can be observed. The intensity of these few modes abruptly weakens and is distributed to other transverse modes; the average spatial beam intensity of the beam profile is increased overall. The output beam has a regular profile and smooth edges. The beam intensity gradually increases from the edge to the center of the beam. There are two peaks in the center of the beam, and the beam intensity distribution resembles double kidneys. Figure 6 shows this process, and a

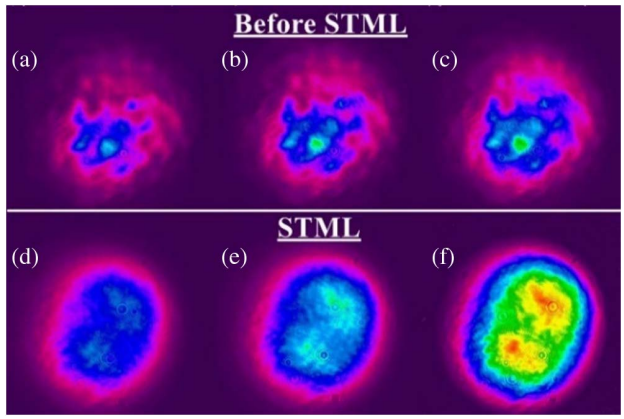

Fig. 6. Beam profile before and during STML by increasing the pump power. The dynamic evolution process is shown in Visualization 1.

more detailed dynamic process is displayed in Visualization 1. It is found that the profile of the output beam is mainly affected by the polarization state. When the state of PC changes, the achieved ML output beam profile varies. It can be explained as follows. In the NPR-based SA, the SA is affected by the state of PC. Since SA has an impact on the evolution of the transverse modes in STML, changing the PC state ultimately leads to a different beam profile. This effect of SA on the output beam profile was also demonstrated in Ref. [7]. During the whole evolution process, the output power of the fiber increases with the change in pump power, as shown in Fig. 2. To the best of our knowledge, nobody has reported this dynamic process before. Although this is the energy evolution process outside the cavity, we think it is of great reference value for understanding and investigating the energy evolution inside the cavity, especially the establishment of STML.

4. CONCLUSION

In this paper, we report an all-fiber STML laser based on long STIN fibers with large modal dispersion for the first time. The experiment and simulation results show that the virtual spatial filtering generated by the insertion of the fiber-based filter plays an important role in the formation of this all-fiber STML laser with large modal dispersion. Through the simple splicing of fibers and adjustment of the PCs, MM mode-locking can be easily achieved when the mode-locking threshold is reached. The measurement of the beam profile, spectrum, and temporal and spatial information before and during mode-locking proves the existence of multiple transverse modes and confirms the generation of STML. In this cavity, when the pump power exceeds 13.7 W, we also observe interesting phenomena that have not been reported before. Furthermore, before and when STML is established, mode intensity dynamic evolution is also observed. We believe it will help to study the establishment of STML and energy evolution between different transverse modes in the cavity. Although there is still room for improvement in output performance, the present results show that it is feasible to use readily available and inexpensive STIN MMF to realize all-fiber STML lasers. In terms of scientific research, the existence of multiple transverse modes in all-fiber STML lasers with large modal dispersion also allows us to observe more complex and high-dimensional physical phenomena. Technically, it also provides a promising method to build an ultra-short pulsed laser with high energy output in an all-fiber system.

APPENDIX A: COMPARISON OF GRIN MMF AND STIN MMF

In this paper, the type of STIN MMF we used is Nufern LMA-YDF-20/125-9M with a 20 μm core diameter and NA = 0.08. The type of GRIN MMF we used is Corning-50/125 with a 50 μm core diameter and NA = 0.2. STIN MMF supports about six modes at 1030 nm, and GRIN MMF supports hundreds of modes. We select the first six modes of the two fibers for simulation calculation, and then obtain the group velocity of STIN MMF and GRIN MMF, as shown in Fig. 7. It can be clearly seen from the figure that compared to GRIN MMF, the high-order mode group velocity of STIN MMF relative to the fundamental mode is much larger than that of GRIN MMF,

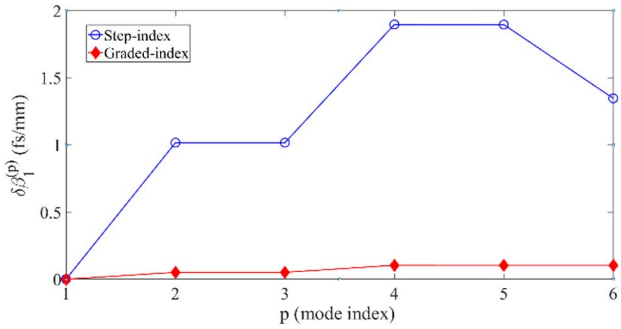

Fig. 7. Comparison of group velocities of the modes of GRIN MMF and STIN MMF relative to the fundamental mode.

about one order of magnitude. Therefore, the modal dispersion in STIN MMF is much greater than that in GRIN MMF.

APPENDIX B: TRANSITION FROM MODE-LOCKING TO Q-SWITCHING MODE-LOCKING

When the laser is operating in the STML, the pulse sequence detected by the oscilloscope is shown in Figs. 2(b) and 2(c). When the pump power exceeds the mode-locking interval, the regular *Q*-switched pulse train can be seen from the oscilloscope as shown in Fig. 8(a), and the repetition rate of the *Q*-switched pulse envelope increases as the pump power increases. The *Q*-switched pulse envelope is turned on at the scale of 200 ns/div, and the period between two ML pulses underneath the envelope is 34.8 ns, corresponding to the light round-trip time in the cavity, as shown in Fig. 8(b).

APPENDIX C: ADDITIONAL SIMULATION DETAILS

To further understand the mode-locking process in the all-fiber cavity, numerical simulations are conducted. The simulation method refers to Ref. [7], where the details can be found. The generalized MM nonlinear Schrödinger equation

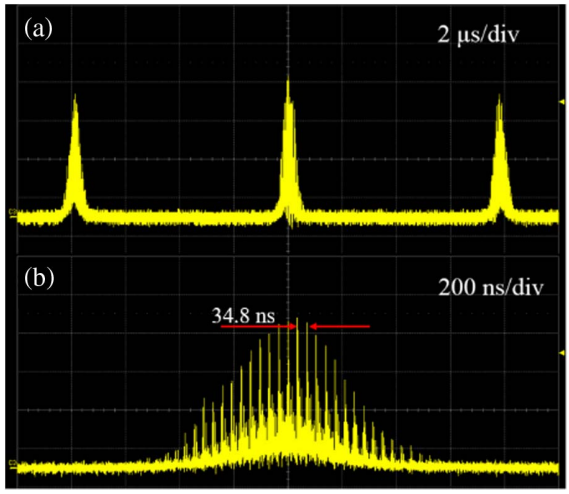

Fig. 8. Pulse sequence recorded by oscilloscope at QSML state with (a) 2 μs/div and (b) 200 ns/div.

(GMMNLSE) is used for the simulation of pulse propagation in passive MMF [20], where the Raman and shock terms are neglected. Modified GMMNLSE with spatially dependent gain saturation is used for the simulation of active MMF. The small-signal gain is 30 dB, the saturation energy of the gain fiber is 8 nJ, and a gain spectrum with a Gaussian profile and 3 dB bandwidth of 40 nm is used. The simulation parameters of MMF are based on the fibers used in the experiments, and the specifications (except for the gain) of the active and passive STIN fibers are set to be the same. The spatial modes, dispersions, and nonlinear coupling coefficients are calculated from the fiber parameters. All six modes in STIN fibers and modes 1–6, 9, 10, 13–15, and 43–45 in GRIN MMF are considered. Since a quasi-SMF is used in the first part of the spectral filter, a virtual spatial filter (i.e., coupling the MM pulse from GRIN MMF to an SMF) is considered, followed by the fiber-based spectral filter, which is modeled as an ideal bandpass filter with a Gaussian profile and a 3 dB bandwidth of 10 nm. Then an instantaneous spatiotemporal SA model is applied, with a saturation power of 16 kW. A lumped loss, including the coupler output loss, of 50% is considered. For the coupling between the GRIN and STIN MMFs, the coupling coefficients are calculated by the overlap integrals among the modes. For the coupling between the GRIN MMF and the quasi-SMF, the coefficients are set to be in proportion [0,0,0,0,0,0,0,0,0,0,0,2,2,9] (which is normalized in the simulations), and for the coupling between the SMF and passive STIN fiber, they are [0,0,0,1,4,7]. Simulations with other coupling coefficients were conducted, and stable mode-locking could also be easily achieved. According to the experimental setup, there is a 0.6 m long passive STIN fiber before the coupler output in Fig. 5.

Funding. Beijing Municipal Natural Science Foundation (4212052); National Natural Science Foundation of China (61735005, 61925010); Fundamental Research Funds for the Central Universities (2021RC206, BUPT2021RC08, 2019JBM069).

Disclosures. The authors declare no conflicts of interest.

Data Availability. Data underlying the results presented in this paper are not publicly available at this time but may be obtained from the authors upon reasonable request.

REFERENCES

1. Z. Wang, L. Li, D. N. Wang, Z. Le, S. Zhang, S. Cao, and Z. Fang, "Generation of pulse-width controllable dissipative solitons and bound solitons by using an all fiber saturable absorber," Opt. Lett. **44**, 570–573 (2019).
2. U. Tegin and B. Ortac, "All-fiber all-normal-dispersion femtosecond laser with a nonlinear multimodal interference-based saturable absorber," Opt. Lett. **43**, 1611–1614 (2018).
3. L. G. Wright, D. N. Christodoulides, and F. W. Wise, "Spatiotemporal mode-locking in multimode fiber lasers," Science **358**, 94–97 (2017).
4. A. Mafi, "Pulse propagation in a short nonlinear graded-index multimode optical fiber," J. Lightwave Technol. **30**, 2803–2811 (2012).
5. U. Tegin, B. Rahmani, E. Kakkava, D. Psaltis, and C. Moser, "Single-mode output by controlling the spatiotemporal nonlinearities in mode-locked femtosecond multimode fiber lasers," Adv. Photon. **2**, 056005 (2020).
6. L. G. Wright, D. N. Christodoulides, and F. W. Wise, "Controllable spatiotemporal nonlinear effects in multimode fibres," Nat. Photonics **9**, 306–310 (2015).
7. Y. Ding, X. Xiao, K. Liu, S. Fan, X. Zhang, and C. Yang, "Spatiotemporal mode-locking in lasers with large modal dispersion," Phys. Rev. Lett. **126**, 093901 (2021).
8. E. Nazemosadat and A. Mafi, "Nonlinear multimodal interference and saturable absorption using a short graded-index multimode optical fiber," J. Opt. Soc. Am. B **30**, 1357–1367 (2013).
9. G. Chen, W. Li, G. Wang, W. Zhang, C. Zeng, and W. Zhao, "Generation of coexisting high-energy pulses in a mode-locked all-fiber laser with a nonlinear multimodal interference technique," Photon. Res. **7**, 187–192 (2019).
10. K. Krupa, A. Tonello, B. M. Shalaby, M. Fabert, A. Barthélémy, G. Millot, S. Wabnitz, and V. Couderc, "Spatial beam self-cleaning in multimode fibres," Nat. Photonics **11**, 237–241 (2017).
11. Z. Liu, L. G. Wright, D. N. Christodoulides, and F. W. Wise, "Kerr self-cleaning of femtosecond-pulsed beams in graded-index multimode fiber," Opt. Lett. **41**, 3675–3678 (2016).
12. E. Deliancourt, M. Fabert, A. Tonello, K. Krupa, A. Desfarges Berthelemot, V. Kermene, G. Millot, A. Barthelemy, S. Wabnitz, and V. Couderc, "Wavefront shaping for optimized many-mode Kerr beam self-cleaning in graded-index multimode fiber," Opt. Express **27**, 17311–17321 (2019).
13. R. Guenard, K. Krupa, R. Dupiol, M. Fabert, A. Bendahmane, V. Kermene, A. Desfarges-Berthelemot, J. L. Auguste, A. Tonello, A. Barthelemy, G. Millot, S. Wabnitz, and V. Couderc, "Kerr self-cleaning of pulsed beam in an ytterbium doped multimode fiber," Opt. Express **25**, 4783–4792 (2017).
14. L. G. Wright, Z. Liu, D. A. Nolan, M. J. Li, D. N. Christodoulides, and F. W. Wise, "Self-organized instability in graded-index multimode fibres," Nat. Photonics **10**, 771–776 (2016).
15. K. Krupa, A. Tonello, A. Barthelemy, V. Couderc, B. M. Shalaby, A. Bendahmane, G. Millot, and S. Wabnitz, "Observation of geometric parametric instability induced by the periodic spatial self-imaging of multimode waves," Phys. Rev. Lett. **116**, 183901 (2016).
16. W. H. Renninger and F. W. Wise, "Optical solitons in graded-index multimode fibres," Nat. Commun. **4**, 1719 (2013).
17. H. Qin, X. Xiao, P. Wang, and C. Yang, "Observation of soliton molecules in a spatiotemporal mode-locked multimode fiber laser," Opt. Lett. **43**, 1982–1985 (2018).
18. Y. Ding, X. Xiao, P. Wang, and C. Yang, "Multiple-soliton in spatiotemporal mode-locked multimode fiber lasers," Opt. Express **27**, 11435–11446 (2019).
19. K. Liu, X. Xiao, Y. Ding, H. Peng, D. Lv, and C. Yang, "Buildup dynamics of multiple-soliton in spatiotemporal mode-locked fiber lasers," Photon. Res. **9**, 1898–1906 (2021).
20. L. G. Wright, Z. M. Ziegler, P. M. Lushnikov, Z. Zhu, M. A. Eftekhar, D. N. Christodoulides, and F. W. Wise, "Multimode nonlinear fiber optics: massively parallel numerical solver, tutorial, and outlook," IEEE J. Sel. Top. Quantum Electron. **24**, 5100516 (2018).
21. H. Wu, W. Lin, Y. J. Tan, H. Cui, Z. C. Luo, W. C. Xu, and A. P. Luo, "Pulses with switchable wavelengths and hysteresis in an all-fiber spatio-temporal mode-locked laser," Appl. Phys. Express **13**, 022008 (2020).
22. X. B. Lin, Y. X. Gao, J. G. Long, J. W. Wu, W. Hong, H. Cui, Z. C. Luo, W. C. Xu, and A. P. Luo, "All few-mode fiber spatiotemporal mode-locked figure-eight laser," J. Lightwave Technol. **39**, 5611–5616 (2021).
23. T. Y. Tsai, Y. C. Fang, H. M. Huang, H. X. Tsao, and S. T. Lin, "Saturable absorber *Q*- and gain-switched all-Yb^{3+} all-fiber laser at 976 and 1064 nm," Opt. Express **18**, 23523–23528 (2010).
24. D. B. Soh, S. E. Bisson, B. D. Patterson, and S. W. Moore, "High-power all-fiber passively *Q*-switched laser using a doped fiber as a saturable absorber: numerical simulations," Opt. Lett. **36**, 2536–2538 (2011).
25. J. Zhou, Y. Lu, B. He, and X. Gu, "*Q*-switched laser in an SMS cavity for inhibiting nonlinear effects," Appl. Opt. **54**, 6080–6084 (2015).

26. W. H. Renninger, A. Chong, and F. W. Wise, "Pulse shaping and evolution in normal-dispersion mode-locked fiber lasers," IEEE J. Sel. Top. Quantum Electron. **18**, 389–398 (2011).
27. A. Mafi, P. Hofmann, C. J. Salvin, and A. Schulzgen, "Low-loss coupling between two single-mode optical fibers with different mode-field diameters using a graded-index multimode optical fiber," Opt. Lett. **36**, 3596–3598 (2011).
28. U. Tegin, B. Rahmani, E. Kakkava, D. Psaltis, and C. Moser, "All-fiber spatiotemporally mode-locked laser with multimode fiber-based filtering," Opt. Express **28**, 23433–23438 (2020).
29. A. Komarov, H. Leblond, and F. Sanchez, "Theoretical analysis of the operating regime of a passively-mode-locked fiber laser through nonlinear polarization rotation," Phys. Rev. A **72**, 063811 (2005).
30. J. W. Wu, Y. X. Gao, X. B. Lin, J. G. Long, H. Cui, Z. C. Luo, W. C. Xu, and A. P. Luo, "*Q*-switched mode-locked multimode fiber laser based on a graphene-deposited multimode microfiber," Chin. Opt. Lett. **19**, 121402 (2021).
31. K. Liu, X. Xiao, and C. Yang, "Observation of transition between multimode *Q*-switching and spatiotemporal mode locking," Photon. Res. **9**, 530–534 (2021).
32. L. Xiaomin, J. Lagsgaard, and D. Turchinovich, "Monolithic highly stable Yb-doped femtosecond fiber lasers for applications in practical biophotonics," IEEE J. Sel. Top. Quantum Electron. **18**, 1439–1450 (2012).
33. C. Aguergaray, N. G. Broderick, M. Erkintalo, J. S. Chen, and V. Kruglov, "Mode-locked femtosecond all-normal all-PM Yb-doped fiber laser using a nonlinear amplifying loop mirror," Opt. Express **20**, 10545–10551 (2012).
34. H. Haig, P. Sidorenko, A. Dhar, N. Choudhury, R. Sen, D. Christodoulides, and F. Wise, "Multimode Mamyshev oscillator," arXiv:2110.03571 (2021).